ACS Sustainable Chemistry & Engineering

pubs.acs.org/journal/ascecg

Research Article

Novel Alcohol Dehydrogenase *Cg*ADH from *Candida glabrata* for Stereocomplementary Reduction of Bulky−Bulky Ketones Featuring Self-Sufficient NADPH Regeneration

Zewen Sun, Jiacheng Zhang, Dejing Yin, Guochao Xu,* and Ye Ni*

Cite This: *ACS Sustainable Chem. Eng.* 2022, 10, 13722−13732

Read Online

ACCESS | Metrics & More | Article Recommendations | Supporting Information

ABSTRACT: Bioreduction of ketones with self-sufficient cofactor regeneration is green and sustainable for the synthesis of chiral secondary alcohols. In this study, a novel alcohol dehydrogenase *Cg*ADH was identified from *Candida glabrata* through genome hunting, exhibiting high oxidation and reduction activities. Conserved motif analysis revealed that *Cg*ADH belongs to the extended SDR subfamily. *Cg*ADH is NADP(H) dependent and displays the highest activity at pH 5.0 and 65 °C. Substrate spectrum analysis indicated that *Cg*ADH exhibited high specificity toward 2-propanol and 2,3-butanediol. Rational engineering of *Cg*ADH was performed to modulate its stereoselectivity in the asymmetric reduction of bulky−bulky ketones. Two stereocomplementary mutants, C244A and V222G/C244N, were obtained with *e.e.* values of 99.6% (*R*) or 94.5% (*S*) toward (4-chlorophenyl)-pyridin-2-ylmethanone, respectively. Moreover, the catalytic efficiency (k_{cat}/K_M) of C244A and V222G/C244N increased by 70- and 25-fold compared with the wild type (WT), respectively. C244A and V222G/C244N also displayed significantly enhanced catalytic efficiency and stereoselectivity toward diaryl ketones with different substituents. Using isopropanol both as a co-substrate and as a co-solvent, a concise self-sufficient NADPH regeneration system was developed to demonstrate the advantage of *Cg*ADH. This study provides evidence of the application potential of the newly identified *Cg*ADH in the preparation of enantiopure diaryl alcohols with low byproducts and E factor.

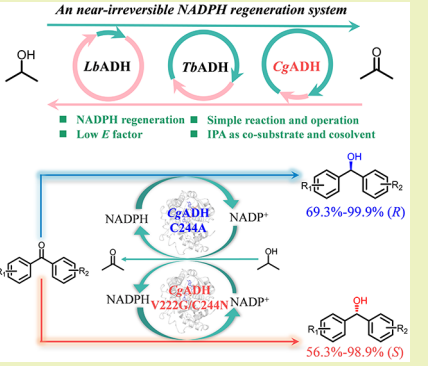

KEYWORDS: *alcohol dehydrogenase, diaryl alcohols, rational engineering, stereocomplementary, concise self-sufficient cofactor regeneration, low waste*

INTRODUCTION

Chiral secondary alcohols are important building blocks for fine chemicals, materials, agrochemicals, food industries, and especially pharmaceuticals.[1] For example, chiral alcohols can serve as motifs of antihistamine, diuretic, antiepileptic, asthma, and antidepressant drugs.[2−4] Ascribing to the gentle reaction conditions, environmental compatibility, high stereoselectivity, and no requirement of complicated protection and deprotection steps, biocatalysts have attracted more and more considerable attention.[5,6] Asymmetric reduction catalyzed by alcohol dehydrogenases (ADHs) or ketoreductases (KREDs) has been increasingly accepted as "*the first choice*" in the synthesis of chiral alcohols due to the high atomic economy and environmental friendliness.[7]

However, the activity of KREDs or ADHs depends on expensive NAD(P)H. In general, when a molecule of chiral alcohol was produced by KREDs or ADH, a molecule of NAD(P)H would be consumed and a molecule of $NAD(P)^+$ would be generated simultaneously (Scheme 1). To reduce the production cost, cofactor regeneration systems, which can be classified into enzyme coupled and substrate coupled according to the dependency on assistant enzymes, should be introduced. Enzyme-coupled systems rely on external co-substrates and assistant enzymes, including formate dehydrogenase, glucose dehydrogenase (GDH), ADH, phosphite dehydrogenase, lactate dehydrogenase and hydrogenase, and so forth, for cofactor regeneration.[8−13] These introduced enzymes usually use their corresponding substrates and $NAD(P)^+$ to generate the same stoichiometric number of reduced coenzyme NAD(P)H. However, these systems were complicated and usually require assistant enzymes and additional devices to maintain pH, which were disadvantageous for the scale-up development in terms of atomic economic and environmental factor (E-factor).[14,15] Substrate-coupled systems refer to the enzymes with dual functions, which could catalyze both the reduction of ketones to the corresponding chiral alcohol and

Received: June 29, 2022
Revised: September 12, 2022
Published: September 30, 2022

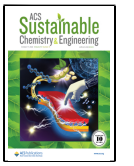

https://doi.org/10.1021/acssuschemeng.2c03872
ACS Sustainable Chem. Eng. 2022, 10, 13722−13732

Scheme 1. Asymmetric Reduction of (4-Chlorophenyl)-pyridin-2-yl-methanone into (*S*)- and (*R*)-CPMA by *Cg*ADH Mutants and Pharmaceuticals with CPMA as the Key Building Block

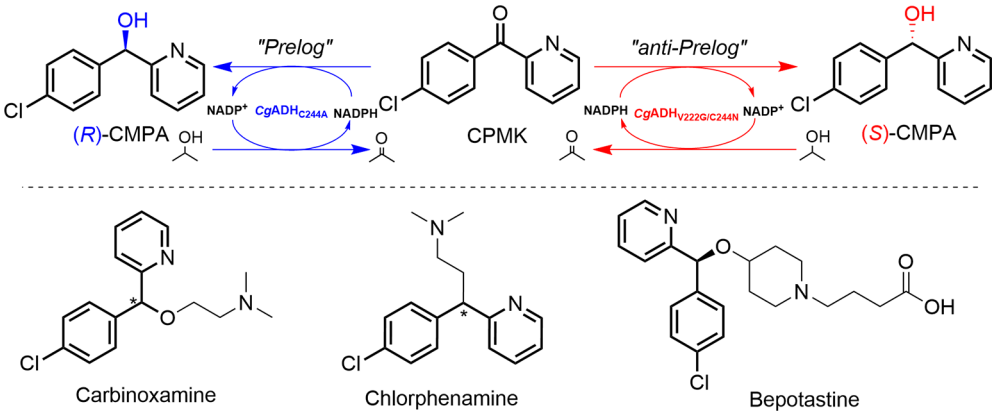

the oxidization of alcohols to the regeneration of coenzymes with the same stoichiometric number. Hence, the substrate-coupled system is neat and self-sufficient without pH changes. Moreover, for the non-natural substrates with low solubility, the co-substrates, such as isopropanol and 1,4-butandiol, could serve as mild co-solvents to enhance the solubility of hydrophobic ketones and avoid duplicated addition of organic co-solvents.[16] Apparently, bioreduction with self-sufficient cofactor regeneration is more promising for green and sustainable chemistry.

Considering the promising application potential in the synthesis of chiral alcohols, several enzymes have been reported and applied in self-sufficient NADH regeneration, such as *Sm*ADH2 from *Stenotrophomonas maltophilia*,[14] *Ls*ADH from *Leifsonia* sp. S749,[17] *Sc*CR from *Streptomyces coelicolor*,[18] and HLADH from horse liver,[19] and so forth. However, few enzymes with self-sufficient NADPH regeneration capability have been identified.[20,21] To the best of our knowledge, *Lb*ADH from *Lactobacillus brevis* and *Tb*ADH from *Thermoanaerobacter brockii* were the two enzymes with self-sufficient NADPH regeneration. NADPH-dependent enzymes were evolutionarily distinct with the NADH-dependent enzymes and usually display a wider substrate spectrum. Hence, identification of novel NADPH-dependent ADHs with self-sufficient cofactor regeneration is of persistent demand.

Genome hunting is an efficient method for identifying novel enzymes from microorganism with industrial relevance.[22] *Candida glabrata*, regarded as an important industrial microorganism, have been proved to be efficient in the asymmetric reduction of aliphatic keto esters and aromatic esters.[23−26] Several reductases have been identified from *C. glabrata*, such as *Cg*KR1 for ethyl (*R*)-*o*-chloromandelate,[27] *Cg*KR2 for ethyl (*R*)-2-hydroxy-4-phenylbutyrate,[28] and *Cg*CR for (*R*)-halohydrins.[29] However, due to their sophisticated spatial structures, biocatalysts usually exhibit strict substrate specificity. There is a continuous demand to develop novel biocatalysts with high activity and stereoselectivity toward non-natural ketones, such as low water-soluble bulky−bulky diaryl ketones.[30−32] Moreover, enantiomers of secondary alcohols could display different or even opposite pharmaceutical effects. For example, (*S*)-4-chloro-3-hydroxybutanoate is the key chiral intermediate for the synthesis of HMG-CoA reductase inhibitor atorvastatin, while (*R*)-4-chloro-3-hydroxybutanoate is applied to the synthesis of L-carnitine.[33] Development of stereocomplementary biocatalysts is of special interests for elucidating the molecular mechanism of stereochemistry and synthesizing of chiral secondary alcohols.

Genome hunting library of *C. glabrata* was constructed to explore KREDs with potentials in the production of chiral alcohols.[34] Cg8 and Cg26 have been identified with a wide substrate scope and high reduction activity based on the average specific activity and Shannon−Wiener index analysis. However, Cg8 and Cg26 could not catalyze the dehydrogenation of alcohols and rely on enzyme-coupled cofactor regeneration systems. In this study, a novel ADH was reported from *C. glabrata* with high oxidation activity toward secondary alcohols and was designated as *Cg*ADH. The enzymatic properties of *Cg*ADH were characterized to facilitate its application. (4-Chlorophenyl)-pyridin-2-yl-methanone (CPMK, **1a**) with low water solubility was chosen as the target to evaluate the application potential of *Cg*ADH. Through the concise engineering, two stereocomplementary mutants were obtained with significantly enhanced activity and stereoselectivity toward **1a** (Scheme 1). These results demonstrate that *Cg*ADH is a promising biocatalyst with self-sufficient substrate-coupled cofactor regeneration capability for the efficient biosynthesis of optically pure alcohols.

EXPERIMENTAL SECTION

Chemical Regents. (4-Chlorophenyl)-pyridin-2-ylmethanone (CPMK) was bought from Heowns Co. Ltd. All other reagents and solvents were of analytical grade, and biochemical reagents were obtained from Sinopharm Chemical Reagent Co. Ltd.

Cloning and Expression of ADHs from *C. glabrata*. Recombinant plasmid pET28a-*Cg*ADH was transformed into *Escherichia coli* BL21(DE3), followed by spreading on a LB plate supplemented with 50 $\mu g \cdot mL^{-1}$ kanamycin and cultivated at 37 °C for 12 h. Positive colony was identified by sequencing and transferred into LB liquid medium with 50 $\mu g \cdot mL^{-1}$ kanamycin and cultivated at 37 °C for 12 h. Then, the final concentration of 1% culture was inoculated into 80 mL of fresh LB medium containing 50 $\mu g \cdot mL^{-1}$ kanamycin and further grown at 37 °C and 120 rpm. When the OD_{600} value reached 0.6−0.8, a final concentration of 0.2 mM IPTG was supplemented for further induction at 25 °C and 120 rpm for 10 h. The cells were collected by centrifugation at 8000 rpm and 4 °C for 5 min, resuspended with sodium phosphate buffer (pH 7.0, 100 mM), and disrupted by ultrasonication. The cell debris was removed by centrifugation at 8000 rpm and 4 °C for 30 min to obtain the crude enzyme extract.

Standard Enzyme Activity Assay Protocol. The standard enzyme activity assay was performed by monitoring the absorbance changes of NADPH at 340 nm. The reaction mixture for reduction

https://doi.org/10.1021/acssuschemeng.2c03872
ACS Sustainable Chem. Eng. 2022, 10, 13722−13732

activity consisted of 1 mM substrate, 0.75 mM NADPH in 190 μL of sodium phosphate buffer (PBS) (pH 6.0, 100 mM), and 10 μL of enzyme solution of appropriate concentration at 30 °C. The reaction mixture for oxidation activity consisted of 5 mM substrate, 1 mM $NADP^+$ in 190 μL of Gly-NaOH (pH 9.5, 100 mM), and 10 μL of enzyme solution of appropriate concentration at 30 °C. OD_{340} was monitored for 3 min, and one unit of enzyme activity (U) was defined as the amount of enzyme required for the consumption or formation of 1 μmol NADPH in 1 min.

Purification of *Cg*ADH. Recombinant *E. coli* BL21(DE3) harboring *Cg*ADH were collected, resuspended in buffer A (20 mM PBS, 0.5 M NaCl, 20 mM imidazole, and pH 7.4), and disrupted twice by high-pressure homogenization at 600−800 bar. The lysates were centrifuged at 12000 rpm and 4 °C for 30 min and filtrated with 0.2 μm filter. The enzymes were purified by a HisTrap affinity column (GE Health care). The fractions containing the target protein were desalted with PBS (100 mM, pH 6.0) using a HiTrap desalting column. Purified enzymes were verified by SDS-PAGE. The concentration of purified *Cg*ADH was measured by Nanodrop 2000c (Thermo Scientific Inc, USA).

Enzyme Characterization of Purified *Cg*ADH. The effects of pH on the reduction and oxidation activities of *Cg*ADH were explored with CPMK (**1a**) or 2-propanol (**1b**) and 0.75 mM NADP(H) as substrates under the above-described conditions except in the following buffers (final concentration 100 mM): sodium citrate (pH 4.0−6.0), sodium phosphate buffer (pH 6.0−8.0), and glycine-NaOH (pH 8.0−10.5) at 30 °C. The effect of temperature on the activity of *Cg*ADH was measured by determining the relative activity toward **1a** at temperature ranges of 25−80 °C in PBS buffer (pH 6.0, 100 mM). Thermostability of *Cg*ADH at sodium phosphate buffer (pH 6.0, 100 mM) was determined by monitoring the residual activity of *Cg*ADH at 30, 40, and 50 °C at different time intervals. In addition, **1a** was used as a standard substrate to test the residual activity of *Cg*ADH using the standard enzyme activity assay protocol. The initial activity was regarded as 100%. All the assays were performed in triplicate.

The effects of various metal ions (including Mn^{2+}, Mg^{2+}, Fe^{3+}, Ca^{2+}, Ni^{2+}, Zn^{2+}, Al^{3+}, Fe^{2+}, Co^{2+}, Cu^{2+}, and Ba^{2+}) and EDTA on the activities of *Cg*ADH were determined by the addition of each reagent into the reaction mixture at 1.0 mM and incubated at 30 °C for 30 min. The residual activities were measured using the standard activity assay protocol. Control experiment was done in the absence of any additives and regarded as 100%. All the experiment was conducted in triplicate.

The specific activities of *Cg*ADH WT toward ketones (**1a**−**12a**) and alcohols (**1b**−**12b**) were investigated by employing the standard activity assay protocol. All the activities were measured in triplicate.

Homology Modeling and Molecular Docking Analysis. The homology model of *Cg*ADH was built based on the crystal structures of holo-Gre2 (PDB ID: 4PVD) and *Cg*KR1 (PDB ID: 5B6K), which shared 53 and 78% sequence identity with *Cg*ADH. Molecular docking was performed using the AutoDock Vina 1.1.2 program. All docking calculations were accomplished with the docking algorithm that took account of ligand flexibility but kept the protein rigid. Docking runs were carried out using the standard parameters of the program for interactive growing and subsequent scoring.

Site-Directed Mutagenesis of *Cg*ADH. Variants were generated by PCR-based site-directed mutagenesis using the recombinant plasmid pET28a-*Cg*ADH as the template, and the corresponding primers are listed in Table S1. The resultant PCR product was digested with *Dpn*I to remove the wild-type *Cg*ADH. Then, the digestion products were transformed into *E. coli* BL21(DE3) using the above-described method.

Determination of Kinetic Parameters. The kinetic parameters were determined using the standard activity assay protocol, except for different concentrations of **1a** (0.2−2.5 mM). The kinetic parameters were calculated according to non-linear curve fitting with Michaelis Menten equation.

Substrate Scopes of *Cg*ADH WT and Variants. For the specific activity analysis, the activity of *Cg*ADH WT and variants toward ketones (**1a** and **13a**−**20a**) were investigated by employing the standard activity assay protocol. All the activities were measured in triplicate. For stereoselectivity analysis, a 1 mL reaction mixture, containing 5 U crude enzyme extract, 10 mM ketones, 0.5 mM $NADP^+$, 20 mM glucose, and 5 U GDHs in PBS buffer (pH 6.0, 100 mM), was employed. The reaction was kept at 30 °C and 120 rpm for 2 h. Then, equal volume of ethyl acetate was added and subjected to vortexing to extract the product. After centrifugation at 12000 rpm for 10 min, the upper organic phase was collected and dried over anhydrous Na_2SO_4 overnight. After centrifugation at 12000 rpm for 10 min, the supernatant was evaporated under vacuum, and equal volume of ethanol was added. Finally, the stereoselectivity of samples was analyzed by HPLC equipped with the Chiralpak IC column (Daicel Chiral Technologies, Co., Ltd.). The detailed analysis methods and retention times are provided in Table S2.

Preparation of (*R*)-CPMA and (*S*)-CPMA by Using *Cg*ADH Variants. A reaction mixture including 10 mL of PBS buffer (pH 7.0, 100 mM), 7 U of cell-free extract of *Cg*ADH C244A, 100 mM (0.217 g) CPMK, and 5% (0.5 mL) 2-propanol was magnetically stirred at 30 °C for the synthesis of (*S*)-CPMA. A reaction mixture including 10 mL of PBS buffer (pH 7.0, 100 mM), 10 U of cell-free extract of *Cg*ADH V222G/C244N, 100 mM (0.217 g) CPMK, 0.5 mM $NADP^+$, and 5% (0.5 mL) 2-propanol was magnetically stirred at 30 °C for the synthesis of (*R*)-CPMA. At different time intervals, samples (100 μL) were withdrawn from the reaction mixture and diluted with 900 μL of PBS buffer (pH 7.0, 100 mM). Equal volume of ethyl acetate immediately was added, thoroughly mixed, and the organic phase was isolated by centrifugation at 12000 rpm for 5 min. The organic phase was dried over anhydrous Na_2SO_4 and analyzed by the HPLC method.

RESULTS AND DISCUSSION

Identification of *Cg*ADH from *C. glabrata* Hunting Library. To facilitate industrial application, ADH with substrate-coupled regeneration is of special interest. Previously, 55 putative short-chain dehydrogenases/reductases (SDRs) were cloned from the genomic DNA of *C. glabrata* and heterologously expressed in *E. coli* BL21(DE3).[34] By screening the SDR library of *C. glabrata*, a novel SDR, namely, Cg31, was identified with relatively high reduction activity toward prochiral ketone, moreover, also with remarkable oxidation activity toward isopropanol (IPA). Cg31 is NADPH dependent and shares a sequence similarity of 78% with *Cg*KR1, a well-studied KRED which is also originated from *C. glabrata*.[35,36] However, *Cg*KR1 could not catalyze the oxidation of alcohols such as IPA. Considering its dual activities, Cg31 was designated as *Cg*ADH.

Multiple sequence alignment of *Cg*ADH and several reported reductases was performed. As shown in Figure S1A, the primary sequence of *Cg*ADH comprises 351 amino acids and possesses the typical cofactor-binding motif at the N-terminal and a catalytic triad composed of S134−Y172−K176. The conserved motifs of *Cg*ADH were analyzed and compared with other SDRs. As shown in Figure S1B, the sequence of the dinucleotide-binding motif in *Cg*ADH, located between β1 and α2, was G14/A15/S16/G17/F18/I19/A20. The sequence of the motif between β3 and α4, conserved for stabilizing the adenine ring of NADP(H), was D64/I65/A66/D67. S16, R39, and K43 could form hydrogen bonds with the phosphate group of NADPH, which endows *Cg*ADH stronger binding affinity toward NADPH than NADH. The catalytic triad locates in the regions of β5 and α7 of *Cg*ADH. It can be seen that all the conserved motifs of *Cg*ADH are consistent with the characteristics of extended SDR subfamily (Figure S1B).[37−39]

Effect of pH, Temperature, and Metal Ion on the Activity of *Cg*ADH. To explore the application potentials of this newly identified *Cg*ADH, enzyme properties were

https://doi.org/10.1021/acssuschemeng.2c03872
ACS Sustainable Chem. Eng. 2022, 10, 13722−13732

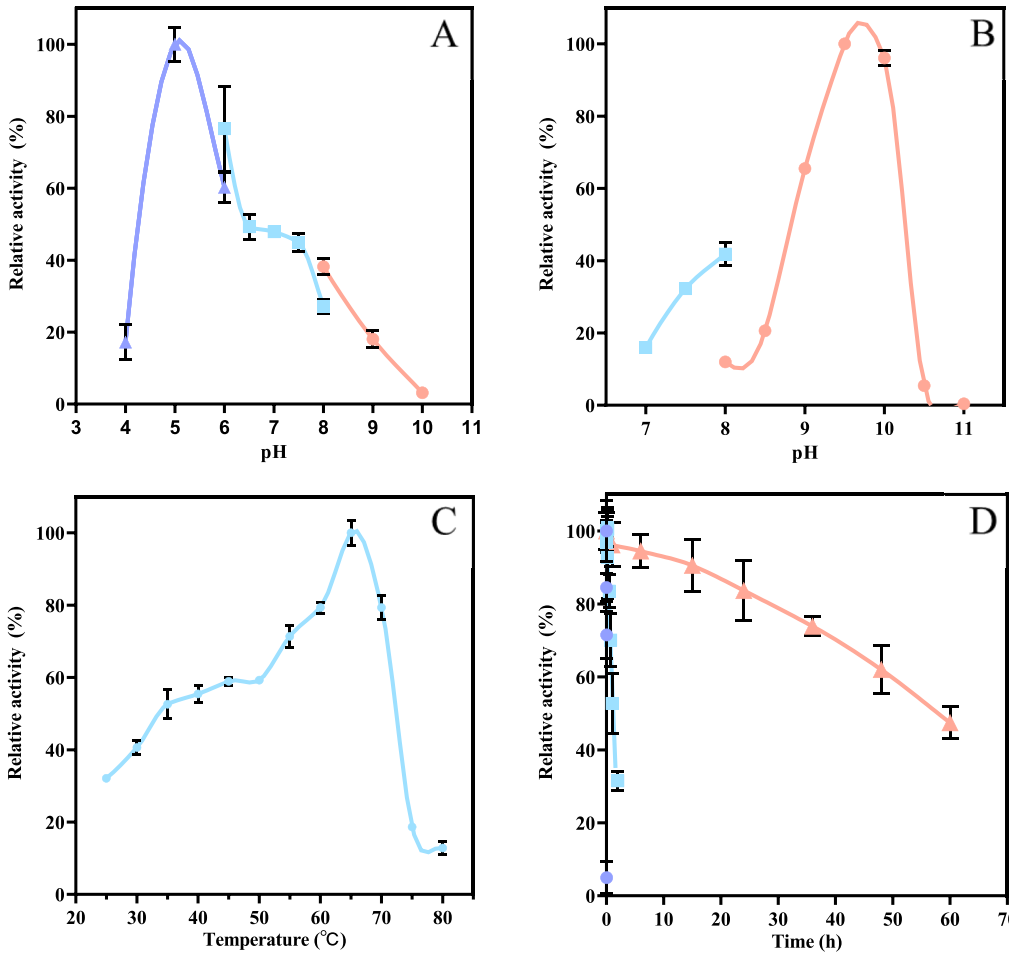

Figure 1. Effect of pH and temperature on reduction and oxidation activities and stability of *Cg*ADH WT. (A) pH activity profile for reduction activity toward **1a**: sodium citrate buffer (pH 4.0−6.0) (blue triangle up solid), sodium phosphate buffer (pH 6.0−8.0) (blue box solid), and glycine−NaOH buffer (pH 9.0−10.0) (pink circle solid). (B) pH activity profile for oxidation activity toward **1b**: sodium phosphate buffer (pH 7.0−8.0) (blue box solid) and glycine−NaOH buffer (pH 9.0−11.0) (pink circle solid). (C) Temperature−activity profile of *Cg*ADH WT; reduction activities of *Cg*ADH were determined with 1.0 mM **1a** in PBS buffer (100 mM, pH 6.0) and at 25−80 °C. (D) Thermostability of *Cg*ADH WT at 30 (pink triangle up solid), 40 (blue circle solid), and 50 °C (blue box solid); purified *Cg*ADH WT was incubated in PBS buffer (100 mM, pH 6.0) at 30−50 °C, and samples were withdrawn at different time intervals for activity assay employing general activity assay protocol.

characterized. *Cg*ADH was purified to electrophoresis purity by nickel-affinity chromatography. The relative molecular mass of *Cg*ADH was estimated to be 39 kDa as indicated by a single band migrated on SDS-PAGE (Figure S2), agreeing with its theoretical molecular weight.

The effects of pH and temperature on the stability and activity of *Cg*ADH were explored (Figure 1). The reduction and oxidation activities were examined with CPMK and isopropanol (IPA) as substrates, respectively. *Cg*ADH displayed the highest reduction activity at pH 5.0. Relative activities at pH 6.0 were determined to be 60.2 and 76.5% of the highest activity in sodium citrate and PBS buffers. The reduction activity decreased sharply in buffers with pH values higher than 7.0 or lower than 5.0. Considering the low stability of NADPH in acidic condition, pH 6.0 was chosen as the compatible pH for further research of *Cg*ADH performance. The optimum pH for oxidation reaction was determined to be pH 9.5. The oxidation activity decreased quickly in buffers with pH values higher than 10.0 or lower than 9.0. The narrow pH range indicates that the pH of reaction could significantly affect the protonation or deprotonation of catalytic residues Tyr172 and influence enzyme activities.

The relative activity of *Cg*ADH was determined over a temperature range from 25 to 80 °C (Figure 1C). The activity of *Cg*ADH gradually increased from 25 to 65 °C and reached the maximum at 65 °C. A further increase in the temperature resulted in a steep decrease in the activity. In order to investigate the thermostability, the half-lives ($t_{1/2}$) of *Cg*ADH were determined by incubating at 30, 40, and 50 °C (Figure 1D). Despite its optimal temperature of 65 °C, *Cg*ADH was not stable at temperatures higher than 40 °C. It was immediately inactivated after incubation at 50 °C for merely 2 min. After incubation at 40 °C for 2 h, *Cg*ADH could retain only about 30% of the initial activity. The $t_{1/2}$ value of *Cg*ADH was calculated to be 55 h at 30 °C according to the Arrhenius deactivation equation. All the above indicates that *Cg*ADH is a mesophilic enzyme.

Influence of metal ions on the activity of *Cg*ADH was explored by incubating the purified *Cg*ADH with various metal ions and EDTA (Figure S3). The relative activities of *Cg*ADH increased to 128% in the presence of Ca^{2+}, while inhibited by Al^{3+}, Cu^{2+}, Fe^{3+}, and Zn^{2+}. Other metal ions had no significant effect on the activity of *Cg*ADH. In the presence of EDTA,

https://doi.org/10.1021/acssuschemeng.2c03872
ACS Sustainable Chem. Eng. 2022, 10, 13722−13732

Table 1. Comparison of *Cg*ADH with Other ADHs with Self-Sufficient NADPH Regeneration

enzyme	length [aa]	metal ion dependence	family	oxidative activity [U·mg^{-1}][a]	reductive activity [U·mg^{-1}][b]	oxd./red.[c]	refs
*Lb*ADH	252	Mg^{2+}	SDR	0.43	3.56	0.12	20
*Tb*ADH	352	Zn^{2+}	MDR	0.93	0.36	2.58	21
*Cg*ADH	351	None	SDR	6.50	1.53	4.25	this study

[a]Oxidative activity toward isopropanol. [b]Reductive activity toward acetone. [c]Oxd./Red. denotes the ratio of oxidative activity to reductive activity.

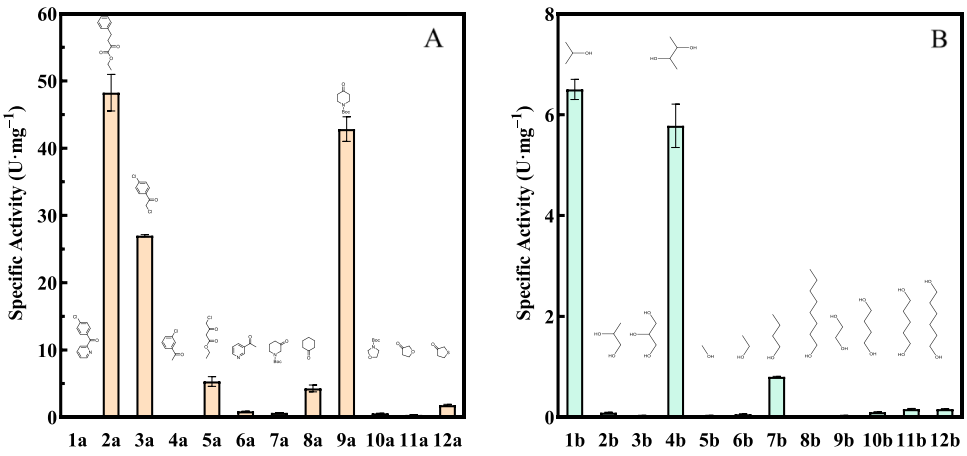

Figure 2. (A) Specific activity of *Cg*ADH WT toward ketones at 30 °C in PBS buffer (100 mM, pH 6.0). (B) Specific activity of *Cg*ADH WT toward alcohols at 30 °C in Gly−NaOH buffer (100 mM, pH 9.5).

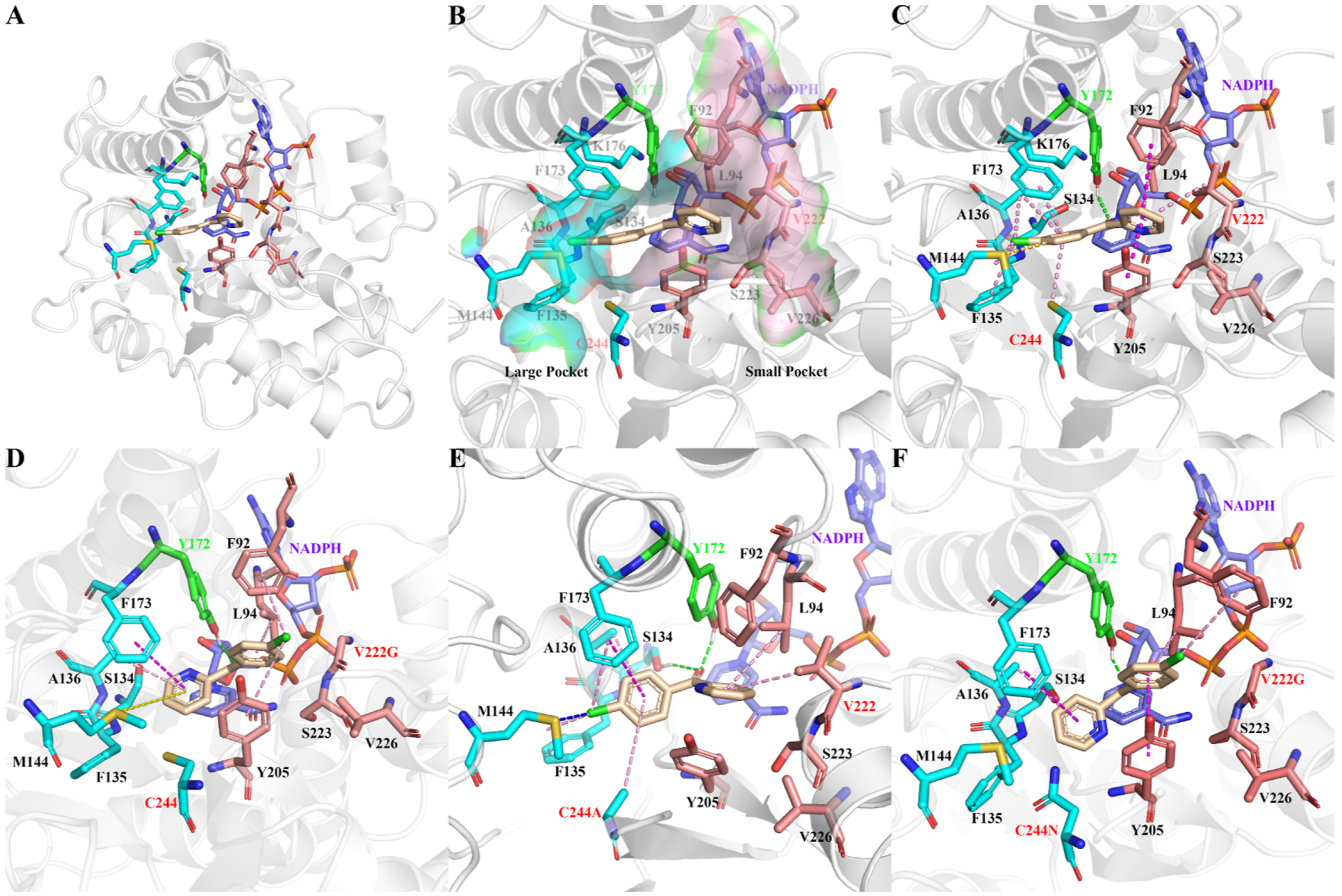

Figure 3. Overview of the residues in the substrate binding pocket of *Cg*ADH. (A) overall structure of WT, (B) enlarged view of large and small binding pocket of WT, (C) substrate interaction analysis of WT, (D) substrate interaction analysis of V222G, (E) substrate interaction analysis of C244A, and (F) substrate interaction analysis of V222G/C244N. Residues in large binding pocket and small binding pocket were depicted in blue and pink, purple: NADPH, green: catalytic Y172, and wheat: CPMK.

https://doi.org/10.1021/acssuschemeng.2c03872
ACS Sustainable Chem. Eng. 2022, 10, 13722−13732

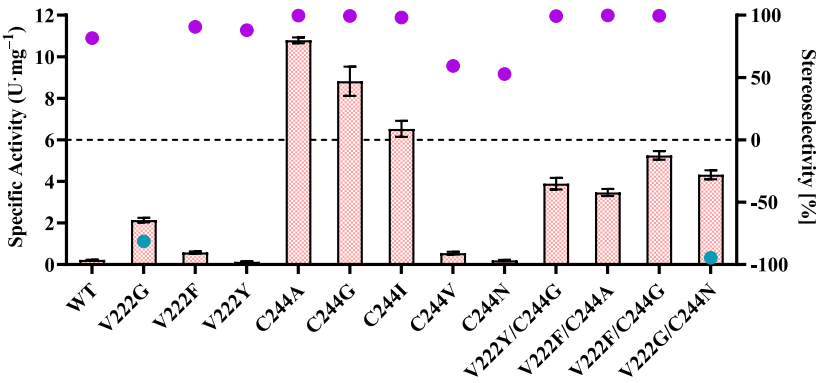

Figure 4. Specific activity and stereoselectivity of *Cg*ADH and variants toward **1a** at 30 °C in PBS buffer (100 mM, pH 6.0). Red grid column: the specific activity of *Cg*ADH and variants toward **1a**. Dot values: the stereoselectivity of *Cg*ADH WT and variants toward **1a**. The blue dot represents the (*R*)-CPMA and the purple dot represents the (*S*)-CPMA. Reactions for stereoselectivity analysis were contained 5 U crude enzyme extract, 10 mM ketones, 0.5 mM $NADP^+$, 20 mM glucose, and 5 U glucose dehydrogenases in PBS buffer (pH 6.0, 100 mM) at 30 °C and 180 rpm for 2 h.

123% residual activity was retained, suggesting that *Cg*ADH is not a metal ion-dependent enzyme.

Comparison of this newly identified *Cg*ADH with *Lb*ADH and *Tb*ADH was performed (Table 1). *Lb*ADH and *Tb*ADH belong to Mg^{2+}-dependent SDR and Zn^{2+}-dependent medium-chain dehydrogenase/reductase (MDR), respectively.[20,21] However, *Cg*ADH was not dependent on any metal ions. The oxidative activity toward isopropanol and the reductive activity toward the acetone of *Lb*ADH were 0.43 and 3.56 U·mg^{-1}, respectively, with an oxidative/reductive ratio of ca. 0.12. The oxidative and reductive activities of *Tb*ADH were 0.93 and 0.36 U·mg^{-1}, respectively, with an oxidative/reductive ratio of ca. 2.58. *Cg*ADH exhibited an oxidative activity of 6.50 U·mg^{-1} and a reductive activity of 1.53 U·mg^{-1}, with an oxidative/reductive ratio of ca. 4.25. The higher oxidative/reductive ratio indicates the decreased reversibility of the self-sufficient NADPH regeneration, which could drive the bioreduction toward the synthesis of chiral alcohols and decrease the loading of isopropanol as a sacrifice co-substrate. As a result, *Cg*ADH is a promising biocatalyst for bioreduction due to its high oxidative activity and oxidative/reductive ratio.

Substrate Spectrum Analysis of *Cg*ADH. The specificity of *Cg*ADH toward ketones and alcohols was investigated. A series of prochiral ketones (**1a**−**12a**) with different substituents and alcohols (**1b**−**12b**) with different chain lengths and hydroxyl positions were tested as substrates. Substrate specificity analysis of ketones provided useful guidance on the application orientation of *Cg*ADH in industrial application. As shown in Figure 2A, *Cg*ADH could catalyze the reduction of all the tested ketones, especially toward the bulky−bulky ketones and cyclic ketones which could only be reduced by few enzymes. Additionally, *Cg*ADH displays great activity with ethyl 2-oxo-4-phenylbutanoate (**2a**), 2,4′-dichloroacetophenone (**3a**), and *N*-(*tert*-butoxycarbonyl)-4-piperidone (**9a**).

As shown in Figure 2B, the oxidative activity of *Cg*ADH was dramatically influenced by the chain length of alcohols. Among various alcohols, the highest activity was 6.50 U·mg^{-1} determined with IPA (**1b**). With regard to methanol (**5b**), ethanol (**6b**), butanol (**7b**), and octanol (**8b**) with different chain lengths, the activity increased accompanied with the increased chain length from methanol to octanol. *Cg*ADH showed relatively lower activity toward diol substrates except 2,3-butanediol (**4b**), suggesting that a second hydroxyl group could interfere with the oxidation activity. *Cg*ADH displayed the second highest activity of 5.78 U·mg^{-1} toward **4b** with merely one methyl difference compared with 1,2-propanediol (**2b**, 0.09 U·mg^{-1}), hinting the favorable effect of methyl group. This newly identified *Cg*ADH could be potentially applied in the preparation of valuable aldehydes ketones and also as a promising cofactor regeneration enzyme.

Rational Engineering the Stereoselectivity of *Cg*ADH toward Diaryl Ketones. Considering *Cg*ADH displaying potential in the reduction of bulky−bulky diaryl ketones, which are generally regarded as "*hard-to-reduce*" substrates, rational engineering of *Cg*ADH was performed for the synthesis of optically pure diaryl alcohols, which are important building blocks in the synthesis of pharmaceuticals. Moreover, *Cg*ADH could utilize IPA to achieve self-sufficient cofactor regeneration, in which IPA is also favorable for increasing the solubility of diaryl ketones. However, the specific activity (0.22 U·mg^{-1}) and stereoselectivity (86.8% (*R*)) toward CPMK of *Cg*ADH were not adequate for scale-up application. As a result, rational engineering was conducted aiming at improving the activity and finely manipulating the stereoselectivity of *Cg*ADH.

The homology model of *Cg*ADH was built based on the crystal structures of *Cg*KR1 from *C. glabrata* (78% identity, PDB: 5B6K) and methylglyoxal/isovaleraldehyde reductase from *Saccharomyces cerevisiae* (53% identity, PDB: 4PVD).[40,41] CPMK (**1a**) was docked into the active center of *Cg*ADH. As shown in Figure 3A−C, CPMK is situated in the active center with the carbonyl group pointing toward the catalytic S134 and Y172 and the carbonyl C atom in a pro-productive state for hydride transfer from NADPH. Further analysis reveals that the chlorophenyl group of CPMK situated in the large binding pocket comprised F135, A136, M144, Y172, F173, and C244, while the pyridyl group of CPMK located in the small binding pocket consisted of L92, F94, V222, S223, Y205, and V226 (Figure 3B). Based on the above analysis, V222 with a moderate volume, a residue at the end of the α8-helix (residues 222−232), might prevent the binding of chlorophenyl group in the small binding pocket. In addition, C244, locating at the end of the β8-sheet (residues 243−248), could assist in the orientation of chlorophenyl group in the large binding pocket. Hence, these two residues were regarded as hotspots in governing the activity and stereoselectivity toward bulky−bulky substrates and were chosen for site-directed mutagenesis.

Saturation mutagenesis of V222 and C244 was performed. The activity and stereoselectivity of beneficial variants toward CPMK were determined as illustrated in Figure 4. Most of the

https://doi.org/10.1021/acssuschemeng.2c03872
ACS Sustainable Chem. Eng. 2022, 10, 13722−13732

Table 2. Kinetic Parameters of *Cg*ADH WT and Variants toward CPMK

enzyme	K_M [mM]	k_{cat} [s^{-1}]	k_{cat}/K_M [$s^{-1}\cdot mM^{-1}$]	fold	*e.e.* [%]/[*R*/*S*]
WT	7.63 ± 2.27	1.32 ± 0.33	0.17	1.0	81.6 (*R*)
C244A	1.78 ± 0.29	22.0 ± 2.0	12.3	71.3	99.6 (*R*)
C244G	3.26 ± 0.56	27.0 ± 3.5	8.27	47.8	99.4 (*R*)
V222Y/C244G	4.75 ± 1.13	15.7 ± 2.9	3.30	19.1	99.2 (*R*)
V222F/C244G	2.14 ± 0.40	11.9 ± 1.4	5.57	32.2	99.8 (*R*)
V222F/C244A	6.68 ± 2.02	19.4 ± 4.7	2.91	16.8	99.5 (*R*)
V222G	2.50 ± 0.26	5.42 ± 0.36	2.17	12.5	81.5 (*S*)
C244N	24.9 ± 3.8	3.75 ± 1.92	0.15	0.9	52.8 (*R*)
V222G/C244N	2.54 ± 0.49	11.1 ± 1.4	4.37	25.7	94.5 (*S*)

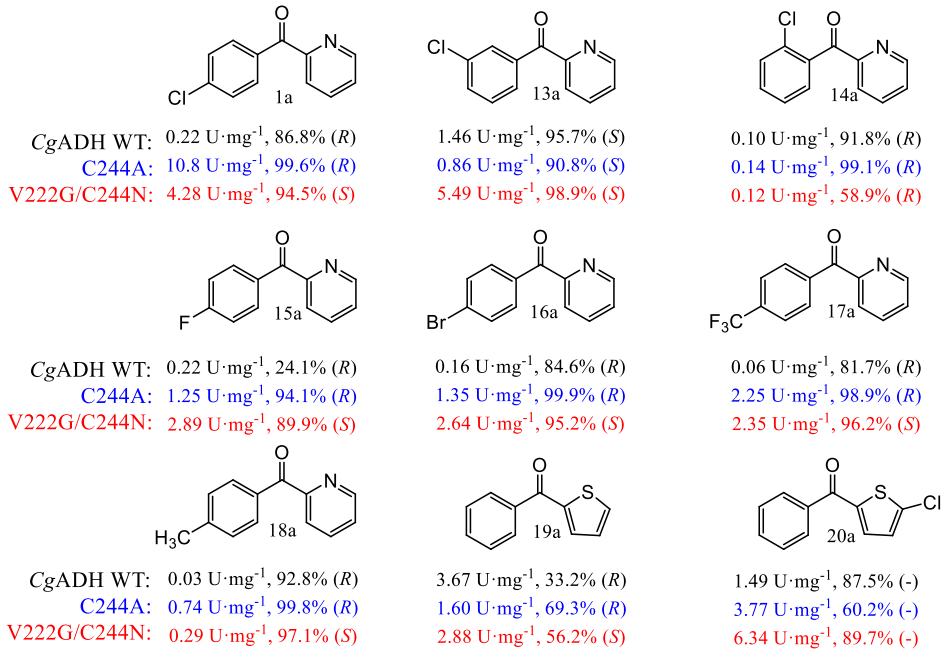

Figure 5. Substrate spectrum of *Cg*ADH and variants toward various prochiral ketones (**1a** and **13a**−**20a**).

mutants of V222 exhibited a similar activity to WT and reversed *S* preference toward CPMK (Table S3). Mutant V222G displayed an *e.e.* value of 81.5% (*S*), reversed with 81.6% (*R*) of WT. Moreover, the activity of V222G was 10-fold of WT. Only two mutants, V222F and V222Y, exhibited enhanced *R*-stereoselectivity. As shown in Figure 3D, it is supposed that the chlorophenyl group of CPMK could be accommodated into the enlarged space of the small binding pocket created by V222G, while for V222F and V222Y, the small binding pocket would be further decreased which is favorable for the location of chlorophenyl group in the large binding pocket. These results indicate that the side chain of residues at site 222 is critical for substrate recognition and orientation. Compared with mutants at position 222, variants at position 244 seemed to have better performance, especially in terms of activity and stereoselectivity. Mutants C244A, C244G, and C244I displayed 29−49 times higher activities than that of WT (0.22 U·mg^{-1}). Remarkably, C244A possessed not only the highest specific activity of 10.8 U·mg^{-1} but also the highest *e.e.* value of 99.6% (*R*). Mutants C244G and C244I also had appreciable performance compared with others. C244N was the only variant of site 244 with the *e.e.* value below 50% (*R*). According to Figure 3E, the smaller side chain of C244A contributes to the enlarged lager binding pocket and creates a new halogen interaction between the chlorophenyl group and M144, which could be accounted for the increased activity and stereoselectivity. However, the small binding pocket is too small to accommodate the chlorophenyl group. Hence, the lowest stereoselectivity was about 50% by single mutation at site 244. Based on docking results, C244A could enhance the activity of *Cg*ADH by decreasing the steric hindrance and improving the binding affinity with chlorophenyl of CPMK in a large binding pocket.

To achieve chiral alcohols with the desirable *R*- and *S*-configurations, combinatorial mutagenesis was further conducted. All single mutations were divided into two groups, one group included the mutants with increased stereoselectivity such as V222Y, V222F, C244A, and C244G and the other group included the mutants with decreased or even reversed stereoselectivity such as V222K, V222G, C244N, and C244V. Then, double mutants were rationally constructed by iteratively combinatorial mutagenesis.

Among all the double mutants with *R*-preference, all of them except V222F/C244A showed compromised activity and stereoselectivity compared with the single-point mutant C244A. As shown in Figure 4, at the expense of a 3-fold decrease in activity, the stereoselectivity of V222F/C244A only increased by 0.2%, representing the highest *e.e.* values of 99.8% (*R*). After the examination of all double mutants with *R*-

https://doi.org/10.1021/acssuschemeng.2c03872
ACS Sustainable Chem. Eng. 2022, 10, 13722−13732

preference, C244A was regarded as the best variant due to its high activity and stereoselectivity and was chosen for further research. For double variants with *S*-preference, stereoselectivities of 52−94% (*S*) toward CPMK were determined. Remarkably, the best variant V222G/C244N gave (*S*)-CPMA with 94.5% *e.e.* and 4.28 U·mg^{-1}, which possessed the highest activity and stereoselectivity with *S*-preference. As shown in Figure 3F, on the basis of V222G, the large binding pocket became narrow by introducing C244N, which lead to the inverted stereoselectivity for the *S*-product. Although the stereoselectivity of (*S*)-selective mutants was not as high as (*R*)-mutants, the stereoselectivity of V222G/C244N is adequate for scale-up application since the optical purity of (*S*)-CPMA could be further enhanced through recrystallization. In summary, under the guidance of rational design, C244A and V222G/C244N were constructed with high activity and stereoselectivity and served for enzyme characterization and evaluation in the synthesis of (*S*)-CPMA and (*R*)-CPMA.

Kinetic Parameter Analysis of *Cg*ADH and Variants. To gain an insight into the effect of substrate binding pockets on the improved stereoselectivity, the kinetic parameter studies of WT *Cg*ADH and beneficial variants were conducted. All variants with over 99% (*R*), the best variant V222G/C244N, and its single point variants were determined. As shown in Table 2, the K_M and k_{cat} values of *Cg*ADH were 7.63 mM and 1.3 s^{-1}, respectively. In the variants with *R*-preference, the variant C244G displayed a high k_{cat}/K_M value of 8.27 s^{-1}·mM^{-1} and the highest k_{cat} value of 27.0 s^{-1}. The best variant C244A exhibited the lowest K_M value and an approximate 70-fold enhanced k_{cat}/K_M value compared with WT. As for variants with *S*-preference, the improvement in activity was not as significant as the *R*-variants. The k_{cat} value of C244N was 3.75 s^{-1}, higher than 1.32 s^{-1} of WT, while its increased K_M led to a lower k_{cat}/K_M of 0.15 s^{-1}·mM^{-1}. V222G not only displayed inverted stereoselectivity but also possessed a lower K_M value of 2.50 s^{-1} and a higher catalytic efficiency k_{cat}/K_M of 5.42 s^{-1}·mM^{-1} compared with WT. Remarkably, the k_{cat}/K_M value of the best *S*-variant V222G/C244N was 4.37 s^{-1}·mM^{-1}, 25-fold of *Cg*ADH, indicating the synergistic effect existed in the double variant V222G/C244N. These results demonstrate that the substitutions at V222 and C244 of *Cg*ADH could significantly influence both the stereoselectivity and activity in the asymmetric reduction of CPMK.

Substrate Spectrum of *Cg*ADH WT and Variants. Various prochiral ketones (**13a−20a**) similar to CPMK were chosen to evaluate the application potential of *Cg*ADH variants in the asymmetric synthesis of chiral bulky−bulky alcohols (Figure 5). Variants showed different activities (0.22−10.8 U·mg^{-1}) toward **1a** and **13a**, whereas all variants showed low activities (below 0.14 U·mg^{-1}) toward **14a**, suggesting that the position of the chloro substituent would affect the substrate binding affinity by interacting with the nearby residues. Comparison of substrates **1a** and **15−18a** shows that the only difference is the types of substituents on the phenyl ring. All variants displayed moderate specific activity (0.78−4.11 U·mg^{-1}) except **18a**. The electronic effects of substituents play a non-negligible role in the activity of *Cg*ADH. The moderate activity of **19−20a** indicates that the pyridyl group would have little effect on the activity. In summary, for CPMK derivatives, the positions of substituents on the phenyl group have great impact on the activity of *Cg*ADH, followed by the polarity of substituents on the phenyl ring; the size of the substituents and the pyridyl group have little effect on the activity.

All *R*- and *S*-variants for CPMK showed *S*-preference toward **13a**. A similar phenomenon was also observed in Chen's research.[42] In addition, variant V222G/C244N displayed slightly reversed selectivity trend in the reduction of **14a**. These results demonstrate that the position of the substituent on the phenyl ring is critical in the stereoselectivity recognition of *Cg*ADH. Consequently, the substrates with different sizes and polarity substituents, such as *para*-fluoride-, *para*-methyl-, *para*-trifluoromethyl-, and *para*-methyl-substituted substrates (**15a**, **16a**, **17a**, and **18a**), were interrogated to test the function of chlorophenyl in the recognition of CPMK. Results show that all variants displayed high stereoselectivity following the original *R*- or *S*-preference toward all *para*-substituent substrates as CPMK, suggesting that the size and electronic factor of substituents in the phenyl group seem to have little influence on stereoselectivity. However, there should be noted that the stereoselectivity of all variants increased slightly with the increasing size of **1a**, **15a**, and **16a**. Finally, 2-benzoylthiophene (**19a**) and (5-chlorothiophen-2-yl)-phenylmethanone (**20a**) were used to investigate the influence of pyridyl group in stereoselectivity. *Cg*ADH WT and variants displayed moderate stereoselectivity toward **19-20a**, demonstrating that the pyridine group of **1a** is indispensable for the orientation of **1a**.

Asymmetric Preparation of Chiral CPMA Employing Variants. To test the advantages of *Cg*ADH variants in scale-up application, a substrate-coupled self-sufficient cofactor regeneration system was developed, in which IPA was served as both hydrogen donor and co-solvent. In traditional enzyme-coupled systems, an assistant enzyme and a co-solvent are required for the reduction of sparingly soluble ketones. The E-factor denotes the amount of waste generated per product equivalent.[43−45] In the reduction of sparingly soluble ketones, such as CPMK, organic solvents were necessary to be added for increasing the mass transferring and promoting the reaction. Hence, the solvents should be taken into account as the waste. For example, in the gram-scale reduction of CPMK with the GDH-coupled cofactor system, both sodium gluconate and organic solvent alcohol should be regarded as waste.[46] The E-factor of the GDH-coupled cofactor system was calculated to be about 264 g·mol^{-1} (1.22 kg·kg^{-1} for CPMA). With regard to this IPA-coupled system, the E-factor was calculated to be only 58 g·mol^{-1} (0.26 kg·kg^{-1} for CPMA), attributed to the low molecular weight of acetone. Moreover, the high oxidative/reductive ratio of *Cg*ADH is conducive to attenuate the reverse reaction of the co-product acetone, which is difficult to achieve using *Lb*ADH and *Tb*ADH (Table 1). Thus, less isopropanol (5%) was added to the reaction. The asymmetric bioreduction reactions were performed using lyophilized crude enzyme of C244A and V222G/C244N. As illustrated in Figure 6, variant C244A could catalyze the asymmetric reduction of 100 mM CPMK with 81.6% isolated yield and 99.6% (*S*) *e.e.* after 2.0 h, and variant V222G/C244N could also efficiently convert 100 mM CPMK into (*S*)-CPMA within 12 h, with 83.3% isolated yield and 94.5% *e.e.*. To the best of our knowledge, this is the first report of enzymatic reduction of a low water-soluble CPMK employing substrate-coupled cofactor regeneration system, with significant advantages of simple reaction system, low cost, and E-factor. These results indicate the practical applications of *Cg*ADH WT

https://doi.org/10.1021/acssuschemeng.2c03872
ACS Sustainable Chem. Eng. 2022, 10, 13722−13732

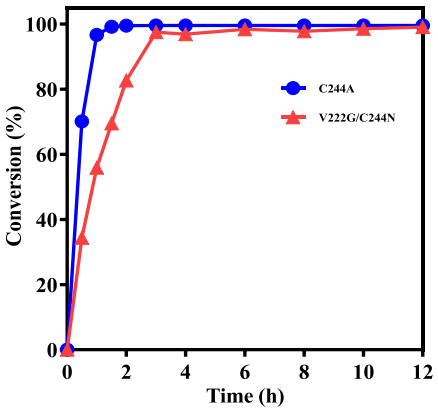

Figure 6. Asymmetric reduction of CPMK through a substrate-coupled cofactor regeneration system employing stereocomplementary variants. Blue circle is the reaction process curve using C244A. Reaction conditions: 9.5 mL of PBS (100 mM, pH 7.0), 7 U of cell-free extract of C244A, 100 mM CPMK, and 0.5 mL of IPA. Red triangle is the reaction process curve using V222G/C244N. Reaction conditions: 9.5 mL of PBS (100 mM, pH 7.0), 10 U of cell-free extract of V222G/C244N, 0.5 mM $NADP^+$, 100 mM CPMK, and 0.5 mL of IPA.

and variants for the preparation of enantiopure alcohols by asymmetric reduction of the corresponding ketones.

CONCLUSIONS

In summary, a novel ADH *Cg*ADH with both reduction and oxidation activity was identified from *C. glabrata*. *Cg*ADH belongs to the NADP(H)-dependent extended SDR subfamily and displays self-sufficient cofactor regeneration capability. To prove its application potential, the stereoselectivity was divergently evolved through a concise design. Two mutants, C244A and V222G/C244N, were obtained, which could produce CPMA with *e.e.* values of 99.6% (*R*) and 94.5% (*S*), respectively. The kinetic parameter and substrate specificity analysis reveal the molecular mechanism of recognition and orientation of bulky−bulky ketones in enzyme and the influence of substrate substituents on the activity and stereoselectivity of enzyme. Moreover, a self-sufficient cofactor regeneration system with C244A and V222G/C244N was developed, and as high as 100 mM CPMK could be completely reduced into (*R*)- and (*S*)-CPMA.

ASSOCIATED CONTENT

Supporting Information

The Supporting Information is available free of charge at https://pubs.acs.org/doi/10.1021/acssuschemeng.2c03872.

Multiple sequence alignment of *Cg*ADH and homologous SDRs, SDS-PAGE analysis of the crude extract and purified *Cg*ADH, effect of metal ions and EDTA on the activity of purified *Cg*ADH, HPLC spectra of *Cg*ADH WT, C244A, and V222G/C244A toward different substrates, primers, HPLC conditions, and specificity and stereoselectivity analysis results (PDF)

AUTHOR INFORMATION

Corresponding Authors

Guochao Xu − *Key Laboratory of Industrial Biotechnology, Ministry of Education, School of Biotechnology, Jiangnan University, Wuxi 214122 Jiangsu, China;* orcid.org/0000-0001-9784-5648; Email: guochaoxu@jiangnan.edu.cn

Ye Ni − *Key Laboratory of Industrial Biotechnology, Ministry of Education, School of Biotechnology, Jiangnan University, Wuxi 214122 Jiangsu, China;* orcid.org/0000-0003-4887-7517; Email: yni@jiangnan.edu.cn

Authors

Zewen Sun − *Key Laboratory of Industrial Biotechnology, Ministry of Education, School of Biotechnology, Jiangnan University, Wuxi 214122 Jiangsu, China*

Jiacheng Zhang − *Key Laboratory of Industrial Biotechnology, Ministry of Education, School of Biotechnology, Jiangnan University, Wuxi 214122 Jiangsu, China*

Dejing Yin − *Key Laboratory of Industrial Biotechnology, Ministry of Education, School of Biotechnology, Jiangnan University, Wuxi 214122 Jiangsu, China*

Complete contact information is available at: https://pubs.acs.org/10.1021/acssuschemeng.2c03872

Author Contributions

CRediT authorship contribution statement. Z. S. contributed to conceptualization, methodology, investigation, and writing—original draft. J. Z. contributed to investigation and methodology. D.Y. contributed to investigation. G.X. contributed to conceptualization, methodology, writing—review and editing, and funding. Y.N. contributed to conceptualization, methodology, writing—review and editing, and funding.

Notes

The authors declare no competing financial interest.

ACKNOWLEDGMENTS

We are grateful to the National Key Research and Development Program (2019YFA0906400), the National Natural Science Foundation of China (22077054 and 22078127), the Open Funding Project of the Key Laboratory of Industrial Biotechnology (KLIB-KF202101), and the Program of Introducing Talents of Discipline to Universities (111-2-06) for the financial support of this research.

REFERENCES

(1) Hollmann, F.; Opperman, D. J.; Paul, C. E. Biocatalytic reduction reactions from a chemist's perspective. *Angew. Chem., Int. Ed. Engl.* **2021**, *60*, 5644−5665.

(2) Bornscheuer, U. T.; Huisman, G. W.; Kazlauskas, R. J.; Lutz, S.; Moore, J. C.; Robins, K. Engineering the third wave of biocatalysis. *Nature* **2012**, *485*, 185−194.

(3) Huisman, G. W.; Liang, J.; Krebber, A. Practical chiral alcohol manufacture using ketoreductases. *Curr. Opin. Chem. Biol.* **2010**, *14*, 122−129.

(4) Zheng, G. W.; Xu, J. H. New opportunities for biocatalysis: driving the synthesis of chiral chemicals. *Curr. Opin. Biotechnol.* **2011**, *22*, 784−792.

(5) Mayr, J. C.; Grosch, J. H.; Hartmann, L.; Rosa, L. F. M.; Spiess, A. C.; Harnisch, F. Resting *Escherichia coli* as chassis for microbial electrosynthesis: production of chiral alcohols. *ChemSusChem* **2019**, *12*, 1631−1634.

(6) Aguirre-Pranzoni, C.; Tosso, R. D.; Bisogno, F. R.; Kurina-Sanz, M.; Orden, A. A. Preparation of chiral *β*-hydroxytriazoles in one-pot chemoenzymatic bioprocesses catalyzed by Rhodotorula mucilaginosa. *Process Biochem.* **2019**, *79*, 114−117.

(7) Yu, S.; Li, H.; Lu, Y.; Zheng, G. A Catalyst from Burkholderia cenocepacia for Efficient Anti-Prelog's Bioreduction of 3,5-Bis-(Trifluoromethyl) Acetophenone. *Appl. Biochem. Biotechnol.* **2018**, *184*, 1319−1331.

(8) Hummel, W. Large-scale applications of NAD(P)-dependent oxidoreductases: recent developments. *Trends Biotechnol.* **1999**, *17*, 487−492.
(9) Nakamura, K.; Yamanaka, R. Light mediated cofactor recycling system in biocatalytic asymmetric reduction of ketone. *Chem. Commun.* **2002**, *16*, 1782−1783.
(10) Kim, Y. H.; Yoo, Y. J. Regeneration of the nicotinamide cofactor using a mediator-free electrochemical method with a tin oxide electrode. *Enzyme Microb. Technol.* **2009**, *44*, 129−134.
(11) Wagenknecht, P. S.; Penney, J. M.; Hembre, R. T. Transition-Metal-Catalyzed Regeneration of Nicotinamide Coenzymes with Hydrogen1. *Organometallics* **2003**, *22*, 1180−1182.
(12) Liu, W. G.; Hu, W. J.; Yang, L. J.; Liu, J. Single cobalt atom anchored on carbon nitride with well-defined active sites for photo-enzyme catalysis. *Nano Energy* **2020**, *73*, 104750.
(13) Weckbecker, A.; Gröger, H.; Hummel, W. Regeneration of nicotinamide coenzymes: principles and applications for the synthesis of chiral compounds. *Adv. Biochem. Eng. Biotechnol.* **2010**, *120*, 195−242.
(14) Yang, Z.; Fu, H.; Ye, W.; Xie, Y.; Liu, Q.; Wang, H.; Wei, D. Efficient asymmetric synthesis of chiral alcohols using high 2-propanol tolerance alcohol dehydrogenase SmADH2 via an environmentally friendly TBCR system. *Catal. Sci. Technol.* **2020**, *10*, 70−78.
(15) Jia, Q.; Zheng, Y. C.; Li, H. P.; Qian, X. L.; Zhang, Z. J.; Xu, J. H. Engineering isopropanol dehydrogenase for efficient regeneration of nicotinamide cofactors. *Appl. Environ. Microbiol.* **2022**, *88*, 15.
(16) Chanquia, S. N.; Huang, L.; García Liñares, G.; Domínguez de María, P.; Kara, S. Deep eutectic solvents as smart cosubstrate in alcohol dehydrogenase-catalyzed reductions. *Catalysts* **2020**, *10*, 1013.
(17) Inoue, K.; Makino, Y.; Dairi, T.; Itoh, N. Gene Cloning and Expression ofLeifsoniaAlcohol Dehydrogenase (LSADH) Involved in Asymmetric Hydrogen-Transfer Bioreduction to Produce (R)-Form Chiral Alcohols. *Biosci. Biotechnol. Biochem.* **2006**, *70*, 418−426.
(18) Wang, L. J.; Li, C. X.; Ni, Y.; Zhang, J.; Liu, X.; Xu, J. H. Highly efficient synthesis of chiral alcohols with a novel NADH-dependent reductase from *Streptomyces coelicolor*. *Bioresour. Technol.* **2011**, *102*, 7023−7028.
(19) Josa-Culleré, L.; Lahdenperä, A. S. K.; Ribaucourt, A.; Höfler, G. T.; Gargiulo, S.; Liu, Y. Y.; Xu, J. H.; Cassidy, J.; Paradisi, F.; Opperman, D. J.; et al. Synthetic biomimetic coenzymes and alcohol dehydrogenases for asymmetric catalysis. *Catalysts* **2019**, *9*, 207−218.
(20) Niefind, K.; Müller, J.; Riebel, B.; Hummel, W.; Schomburg, D. The crystal structure of *R*-specific alcohol dehydrogenase from *Lactobacillus brevis* suggests the structural basis of its metal dependency. *J. Mol. Biol.* **2003**, *327*, 317−328.
(21) Ju, S. Y.; Qian, M. X.; Li, J.; Xu, L. R.; Yang, J. P.; Wu, J. A biocatalytic redox cascade approach for one-pot deracemization of carboxyl-substituted tetrahydroisoquinolines by stereoinversion. *Green Chem.* **2019**, *21*, 5579−5585.
(22) Ni, Y.; Xu, J. H. Biocatalytic ketone reduction: A green and efficient access to enantiopure alcohols. *Biotechnol. Adv.* **2012**, *30*, 1279−1288.
(23) Wang, J. P.; Cheng, P. F.; Wu, Y. F.; Wang, A. M.; Liu, F. M.; Pei, X. L. Discovery of a new NADPH-dependent aldo-keto reductase from *Candida orthopsilosis* catalyzing the stereospecific synthesis of (*R*)-pantolactone by genome mining. *J. Biotechnol.* **2019**, *291*, 26−34.
(24) Li, S. B.; Liu, L. M.; Chen, J. Compartmentalizing metabolic pathway in *Candida glabrata* for acetoin production. *Metab. Eng.* **2015**, *28*, 1−7.
(25) Li, Y.; Chen, J.; Lun, S. Y. Biotechnological production of pyruvic acid. *Appl. Microbiol. Biotechnol.* **2001**, *57*, 451−459.
(26) Liu, J. Y.; Zheng, G. W.; Li, C. X.; Yu, H. L.; Pan, J.; Xu, J. H. Multi-substrate fingerprinting of esterolytic enzymes with a group of acetylated alcohols and statistic analysis of substrate spectrum. *J. Mol. Catal. B Enzym.* **2013**, *89*, 41−47.
(27) Ma, H. M.; Yang, L. L.; Ni, Y.; Zhang, J.; Li, C. X.; Zheng, G. W.; Yang, H. Y.; Xu, J. H. Stereospecific Reduction of Methyl o-Chlorobenzoylformate at 300 g·L−1 without Additional Cofactor using a Carbonyl Reductase Mined from Candida glabrata. *Adv. Synth. Catal.* **2012**, *354*, 1765−1772.
(28) Shen, N. D.; Ni, Y.; Ma, H. M.; Wang, L. J.; Li, C. X.; Zheng, G. W.; Zhang, J.; Xu, J. H. Efficient synthesis of a chiral precursor for angiotensin-converting enzyme (ACE) inhibitors in high space-time yield by a new reductase without external cofactors. *Org. Lett.* **2012**, *14*, 1982−1985.
(29) Xu, G. C.; Yu, H. L.; Shang, Y. P.; Xu, J. H. Enantioselective bioreductive preparation of chiral halohydrins employing two newly identified stereocomplementary reductases. *RSC Adv.* **2015**, *5*, 22703−22711.
(30) Qu, G.; Liu, B. B.; Jiang, Y. Y.; Nie, Y.; Yu, H. L.; Sun, Z. T. Laboratory evolution of an alcohol dehydrogenase towards enantioselective reduction of difficult-to-reduce ketones. *Bioresour. Bioprocess.* **2019**, *6*, 8.
(31) Liu, B. B.; Qu, G.; Li, J. K.; Fan, W. C.; Ma, J. A.; Xu, Y.; Nie, Y.; Sun, Z. T. Conformational Dynamics-Guided Loop Engineering of an Alcohol Dehydrogenase: Capture, Turnover and Enantioselective Transformation of Difficult-to-Reduce Ketones. *Adv. Synth. Catal.* **2019**, *361*, 3182−3190.
(32) Qu, G.; Bi, Y. X.; Liu, B. B.; Li, J. K.; Han, X.; Liu, W. D.; Jiang, Y. Y.; Qin, Z. M.; Sun, Z. T. Unlocking the Stereoselectivity and Substrate Acceptance of Enzymes: Proline-Induced Loop Engineering Test. *Angew. Chem. Int. Ed.* **2022**, *61*, 8.
(33) Ha, T. H.; Suh, K. H.; Lee, G. S. A Novel synthetic method for Bepotastine, a histamine H1 receptor antagonist. *Bull. Korean Chem. Soc.* **2013**, *34*, 549−552.
(34) Xu, G.; Zhang, Y.; Wang, Y.; Ni, Y. Genome hunting of carbonyl reductases from *Candida glabrata* for efficient preparation of chiral secondary alcohols. *Bioresour. Technol.* **2018**, *247*, 553−560.
(35) Huang, L.; Xu, J. H.; Yu, H. L. Significantly improved thermostability of a reductase CgKR1 from Candida glabrata with a key mutation at Asp 138 for enhancing bioreduction of aromatic α-keto esters. *J. Biotechnol.* **2015**, *203*, 54−61.
(36) Zheng, G. W.; Liu, Y. Y.; Chen, Q.; Huang, L.; Yu, H. L.; Lou, W. Y.; Li, C. X.; Bai, Y. P.; Li, A. T.; Xu, J. H. Preparation of structurally diverse chiral alcohols by engineering ketoreductase CgKR1. *ACS Catal.* **2017**, *7*, 7174−7181.
(37) Kavanagh, K. L.; Jörnvall, H.; Persson, B.; Oppermann, U. Medium- and short-chain dehydrogenase/reductase gene and protein families. *Cell. Mol. Life Sci.* **2008**, *65*, 3895−3906.
(38) Persson, B.; Kallberg, Y.; Bray, J. E.; Bruford, E.; Dellaporta, S. L.; Favia, A. D.; Duarte, R. G.; Jörnvall, H.; Kavanagh, K. L.; Kedishvili, N.; Kisiela, M.; Maser, E.; Mindnich, R.; Orchard, S.; Penning, T. M.; Thornton, J. M.; Adamski, J.; Oppermann, U. The SDR (short-chain dehydrogenase/reductase and related enzymes) nomenclature initiative. *Chem. Biol. Interact.* **2009**, *178*, 94−98.
(39) Breicha, K.; Müller, M.; Hummel, W.; Niefind, K. Crystallization and preliminary crystallographic analysis of Gre2p, an NADP+-dependent alcohol dehydrogenase fromSaccharomyces cerevisiae. *Acta Crystallogr., Sect. F: Struct. Biol. Cryst. Commun.* **2010**, *66*, 838−841.
(40) Qin, F.; Qin, B.; Mori, T.; Wang, Y.; Meng, L.; Zhang, X.; Jia, X.; Abe, I.; You, S. Engineering of Candida glabrata Ketoreductase 1 for Asymmetric Reduction of α-Halo Ketones. *ACS Catal.* **2016**, *6*, 6135−6140.
(41) Guo, P. C.; Bao, Z. Z.; Ma, X. X.; Xia, Q.; Li, W. F. Structural insights into the cofactor-assisted substrate recognition of yeast methylglyoxal/isovaleraldehyde reductase Gre2. *Biochim. Biophys. Acta* **2014**, *1844*, 1486−1492.
(42) Li, Z.; Wang, Z.; Wang, Y.; Wu, X.; Lu, H.; Huang, Z.; Chen, F. Substituent Position-Controlled Stereoselectivity in Enzymatic Reduction of Diaryl- and Aryl(heteroaryl)methanones. *Adv. Synth. Catal.* **2019**, *361*, 1859−1865.
(43) Sheldon, R. A. The E factor 25 years on: the rise of green chemistry and sustainability. *Green Chem.* **2017**, *19*, 18−43.
(44) Tieves, F.; Tonin, F.; Fernández-Fueyo, E.; Robbins, J. M.; Bommarius, B.; Bommarius, A. S.; Alcalde, M.; Hollmann, F.

https://doi.org/10.1021/acssuschemeng.2c03872
ACS Sustainable Chem. Eng. 2022, 10, 13722−13732

Energising the E-factor: The E+-factor. *Tetrahedron* **2019**, *75*, 1311−1314.
(45) Ni, Y.; Holtmann, D.; Hollmann, F. How green is biocatalysis? To calculate is to know. *ChemCatChem* **2014**, *6*, 930−943.
(46) Xu, G. C.; Wang, Y.; Tang, M. H.; Zhou, J. Y.; Zhao, J.; Han, R. Z.; Ni, Y. Hydroclassified Combinatorial Saturation Mutagenesis: Reshaping Substrate Binding Pockets of KpADH for Enantioselective Reduction of Bulky-Bulky Ketones. *ACS Catal.* **2018**, *8*, 8336−8345.

https://doi.org/10.1021/acssuschemeng.2c03872
ACS Sustainable Chem. Eng. 2022, 10, 13722−13732